A NEW METHODOLOGY FOR THE ACOUSTIC DESIGN OF COMPRESSION DRIVER PHASE-PLUGS WITH CONCENTRIC ANNULAR CHANNELS

M Dodd Celestion International Ltd, Ipswich, IP6 0NL, UK
J Oclee-Brown ISVR, University of Southampton, S017 1BJ, UK
KEF Audio (UK) Ltd, Maidstone, ME15 6QP

1 INTRODUCTION

Compression drivers couple a radiating membrane to a horn throat of smaller area. When coupled to a suitable horn, this area reduction improves the match between the mechanical impedance of the driver and the acoustic radiation impedance. This improved impedance matching results in efficiencies far higher than those produced by direct radiators.

Early workers[1] found that achieving this high compression ratio required the cavity between horn throat and membrane to be 'plugged' reducing the air volume and high frequency loss due to its compliance. Further improvement at high-frequencies could be made by splitting the sound path between membrane and throat into a number of channels of equal length and of smoothly increasing area. These devices soon became known as ‘phase-plugs’ since they were intended to correct the phase by providing paths of equal length from the membrane to the horn throat thus avoiding destructive interference. Phase-plugs allow large membranes and correspondingly large voice coils to be used with directional horns yielding a massive increase in maximum SPL when compared to an equivalent direct radiating loudspeaker.

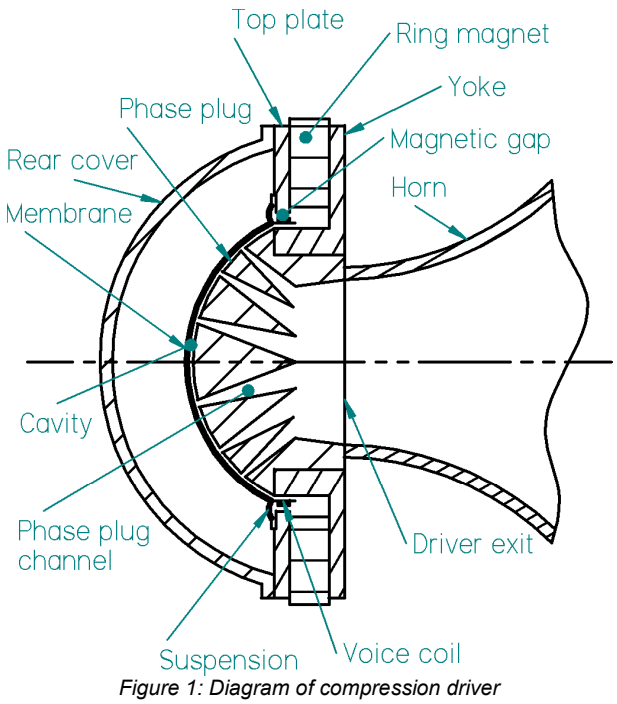

Figure 1: Diagram of compression driver

Poorly designed phase-plugs exhibit large response irregularities which often limit driver performance.

In this paper we firstly explore 'equal path-length' and 'modal' methods of phase-plug design on an idealized model with a cylindrical air cavity and planar rigid piston using the Finite Element Method

(FEM). We will then compare this flat disc shaped cavity to a more realistic spherical cap shaped cavity. A new methodology for the positioning and sizing of annular phase-plug channels is then presented.

1.1 Compression Driver Description

Figure 1 shows a schematic section through a typical compression driver with annular channel phase-plug. The ring magnet produces an intense magnetic field that is concentrated in the magnetic gap by the highly permeable top plate and yoke. The voice coil is immersed in this strong radial field, current flowing in it results in an axial force. This force is transmitted to the membrane by a rigid former. A flexible suspension maintains the centralization of the coil, while allowing axial motion. Axial displacement of the membrane causes the cavity width to be reduced, resulting in an airflow down the channels, through the driver exit and into the horn. In the driver considered in this paper, the magnetic gap is filled with magnetic fluid. This simplifies the acoustic behaviour by blocking the air cavity in the magnet.

1.2 FEM Methodology

The geometries being considered in this paper are all axisymmetric and orientated with the x-axis being the axis of rotational symmetry. To take advantage of this symmetry in the analysis, second-order axisymmetric elements are used throughout.

The models of idealized compression-driver membranes are represented with shell elements, having repeated freedoms and restraints to replicate rigid body motion. The air is represented by 'solid' quadrilateral elements. The termination of the channels is achieved by applying the specific impedance of air as a boundary condition to the channel ends. This avoids reflections as the channels are narrow compared to a wavelength and only plane waves can propagate within them. The effects of viscosity are neglected in these models.

The models of idealised compression drivers have a constant force applied to the membrane, whereas the models of the cavity only have the membrane constrained to move a fixed displacement.

The FEM examples of idealized drivers have a moving mass of 0.04 gram, with 1N of driving force is applied. All models have a 80mm diameter membrane with cavity width of 0.3mm and a compression ratio, which is the ratio of total channel area to membrane area, of 15.

The solutions are obtained with the PAFEC[2] linear sinusoidal solver running on an Intel Xeon 2.33Ghz processor. For the idealized compression drivers this allows 500 frequencies to be solved in approximately 20 seconds.

The idealised driver models are solved to obtain the pressure frequency responses at selected points near the channel end. For our purposes, the aim is to have smooth responses with the same pressure in all channels.

Contour plots of the pressure in the cavity as a function of frequency and position are produced to illustrate the pressure behaviour in the cavity.

2 CURRENT PHASE-PLUG DESIGN METHODS

2.1 Equal Path Length Approach

One of the earliest concepts applied to positioning the channels in a phase-plug results from considering the effect of destructive interference. If we assume that the sound simply travels from a point on the membrane to the nearest channel then we can consider the path lengths from the membrane to the desired wavefront. It would then seem reasonable to assume that where the

shortest and longest path lengths are half a wavelength we could expect destructive inference to occur. This leads to the conclusion that if we position the channels to keep the path length differences to less than a quarter of a wavelength of the highest frequency in the desired bandwidth then we could expect a good response up to this frequency[3].

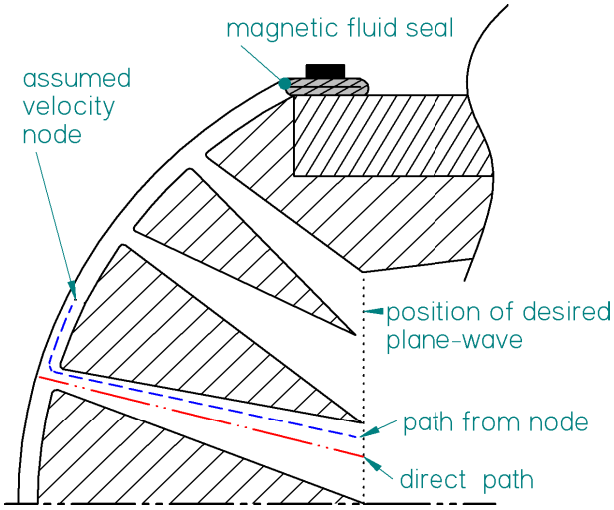

Figure 2: Detail of compression driver showing path lengths from membrane to position of desired wavefront.

To explore this idea further we will consider the results of a FEM model of an idealized version of the compression driver shown in Figure 2. Compression drivers with magnetic fluid in the gap fit the idealized model best since the fluid may be assumed to remain stationary. The resulting acoustical seal, shown in Figure 2, prevents sound leakage out of the cavity between membrane and phase-plug.

The idealized driver, shown in Figure 3, has three channels and circular planar piston. The piston is constrained to move as a rigid body and forms one face of the cylindrical cavity. The other face has the three equally spaced annular channels terminated with an appropriate impedance to avoid reflections.

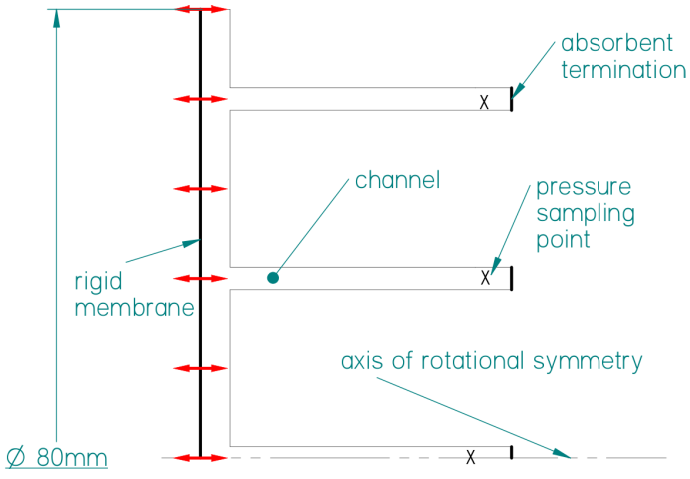

Figure 3: Geometry used for FEM model with three evenly spaced channels

The path length difference between longest and shortest path is 16mm, which is half a wavelength at 10.625kHz (ka=7.7). The results of the FEM analysis are shown in Figure 4, the pressure in the three channels is plotted.

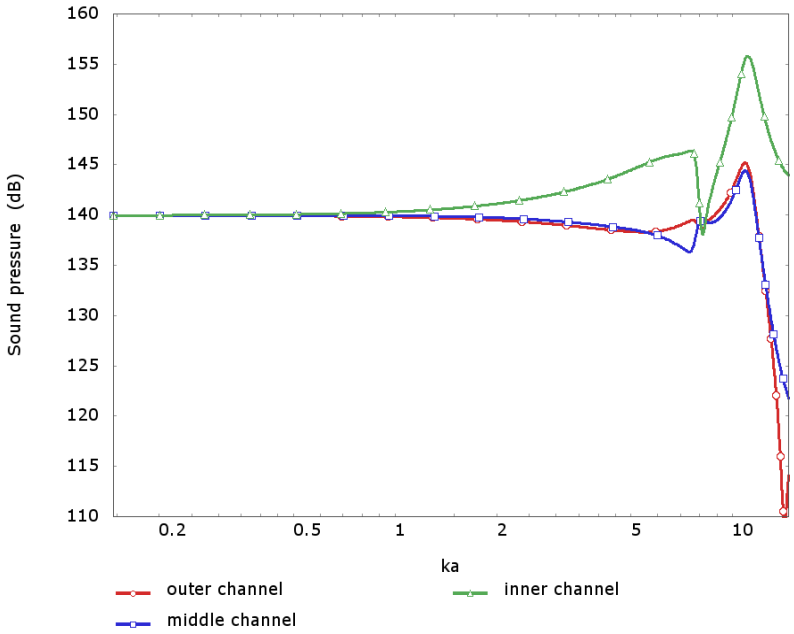

Figure 4: Pressure response of cylindrical cavity with equal channel widths and equal path length.

It may be observed that these pressures are not regular and do not all have dips at 10.6kHz (ka=7.7) as one may expect. Additionally, some severe peaks are present in the response that cannot be readily explained by path length difference and interference.

2.2 Modal Control by Channel Balancing

When a phase-plug is placed in front of the radiating membrane, a thin cavity is created. The response irregularities observed in section 2.1 are due to excitation of acoustic resonances in this cavity.

The nature of these resonances can be clearly demonstrated if the same cavity as analysed above, with channels removed, is driven by a source at its outside diameter. Figure 5 shows a contour plot the pressure variation across the cavity radius (vertical axis) with frequency (horizontal axis) calculated by an FEM model for this case.

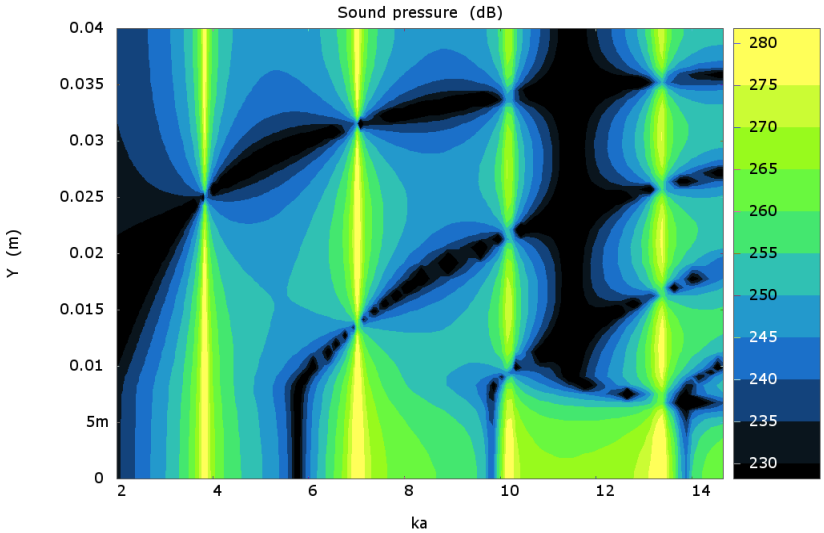

Figure 5: Pressure variation in cavity with source at outside diameter.

An interesting solution exists when the same cylindrical cavity with no channels is driven by a circular planar rigid membrane on one of its faces. The piston is constrained to move with a fixed displacement to avoid pressure variation with frequency. The pressure variation across the cavity radius is displayed as a contour in Figure 2. There is a maximum of 0.002dB variation across the entire cavity.

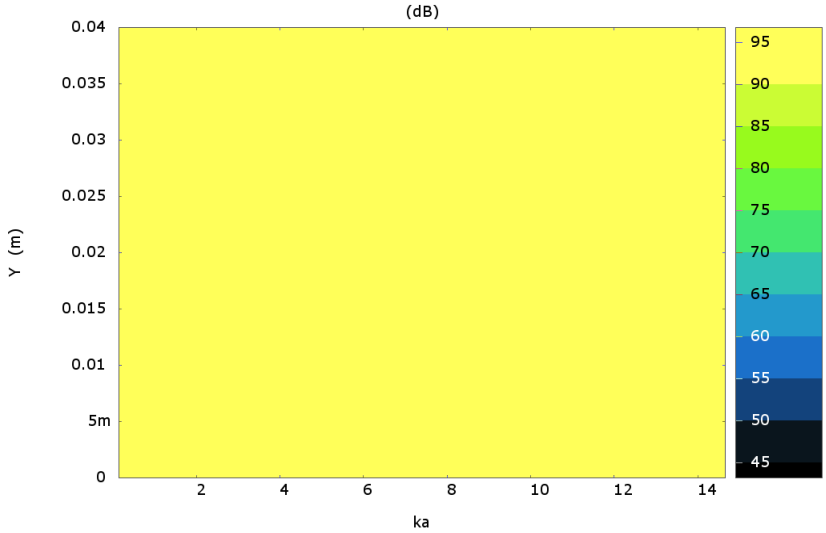

Figure 6: Planar piston in cylindrical cavity. No contours since pressure variation only 0.002dB.

There is no modal excitation since axially the cavity is much smaller than a wavelength, even at the highest frequency considered, and the radial modes are not excited as they are driven orthogonally.

From this result we may now conclude that, in the case of the evenly spaced channels, discussed in section 2.1, it is the loading of the channels that excites the cavity modes.

2.2.1 Suppression of Modes by Channel Position and Size

Smith[4] shows that it is possible, in this simplified cylindrical representation, to choose the areas and radii of the N channels so that the modal excitation from each cancels for modes up to the Nth mode. An example of such a design is illustrated by Murray[5].

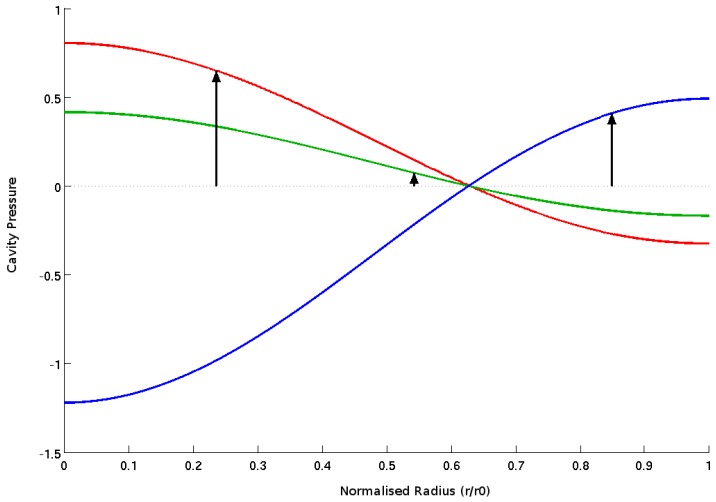

Figure 7: Pressure excited by each channel plotted against normalized radius for the first mode.

Figure 7 shows the excitation of the first radial cavity mode by each of three phase-plug channels positioned as described by Smith. The three modal excitations, due to the presence of each channel, sum to zero and the mode is suppressed.

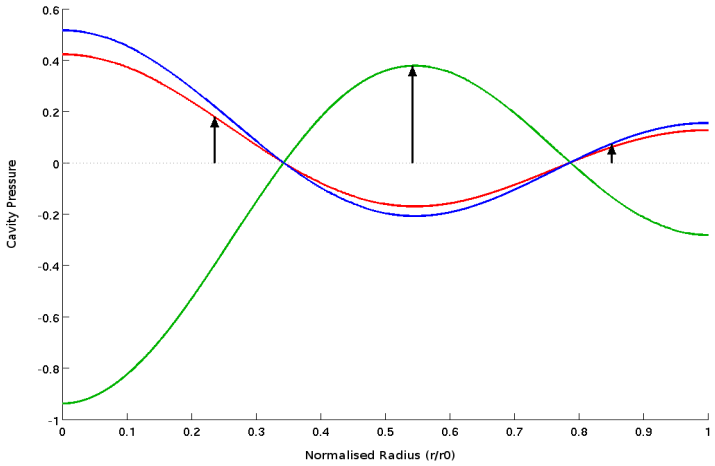

Figure 8: Pressure excited by each channel plotted against normalized radius for the second mode.

Figure 8 displays the same information, this time for the second radial cavity mode. The degree to which each channel excites the mode is dependent upon the channel area and also the magnitude of the mode at the channel position, this is why the magnitude of excitation from each channel is not the same in the two plotted cases.

The third radial mode is also suppressed, though, this is not plotted as it is a trivial result - each channel is positioned at a nodal line and each provides no contribution to the modal excitation.

The vectors show the excitation of the modes at the channel positions. In all three cases, at any position in the cavity, the pressure cancels resulting in zero modal excitation.

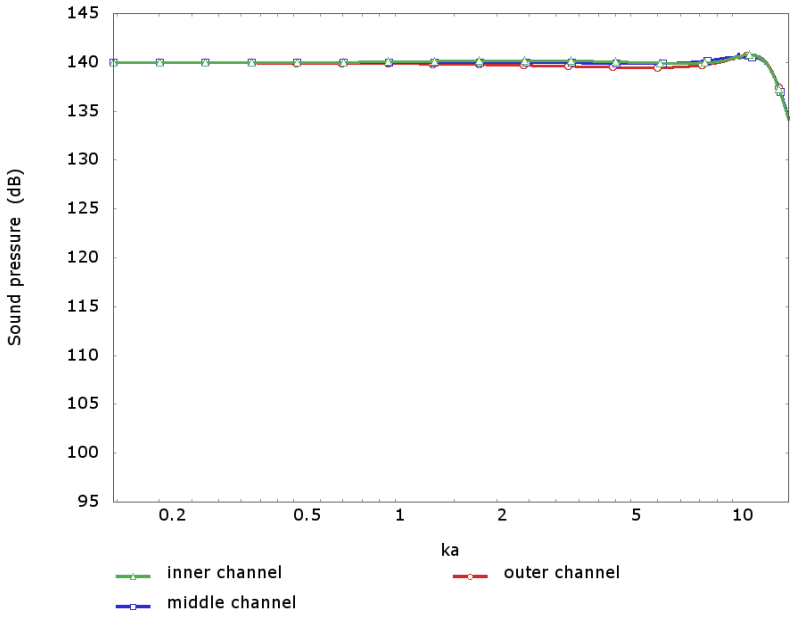

Figure 9: Channel pressure response of planar piston compression driver with phase-plug design to suppress cavity resonances using Bob Smith method.

Figure 9 shows the pressure response of each channel calculated by an FEM model of a three channel Smith phase-plug. The channel pressures are almost identical confirming the almost complete absence of cavity modes.

2.2.2 The Effect of Practical Departure from a Cylindrical Geometry

In practice compression driver membranes need curvature to be sufficiently rigid and are shaped as a spherical cap. The more curved the membrane the higher the first parasitic structural mode.

The effect of this departure from the simplified cylindrical geometry cannot be neglected: the motion of the membrane is no longer orthogonal to the cavity resonances.

Figure 10 shows that an axially moving spherical cap will excite resonances in the, now curved, compression cavity. The positions and ratios calculated by Smiths analysis will not suppress this modal excitation.

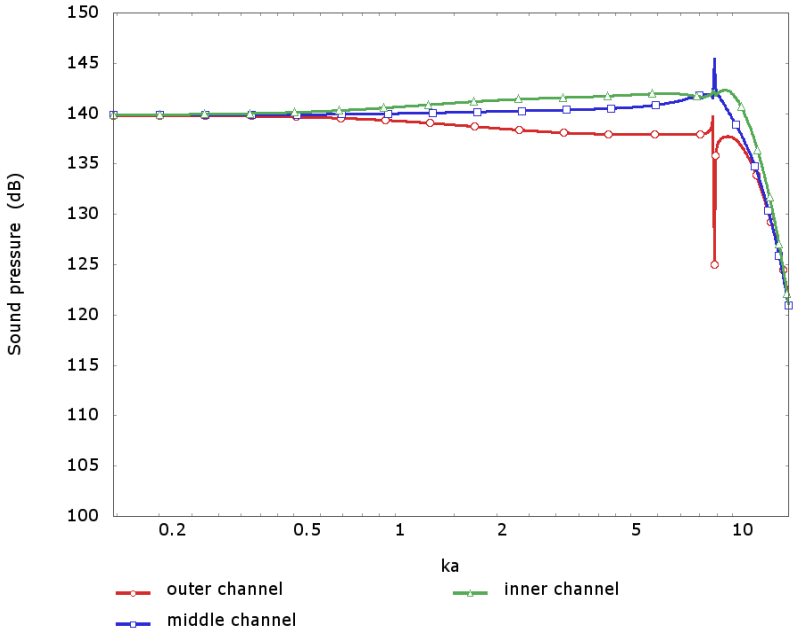

Figure 10: Channel pressure response of spherical cap piston compression driver with phase-plug design to suppress cavity resonances using Bob Smith method.

3 MODAL EXCITATION BY MEMBRANE

The important aspect of the behaviour that is overlooked by an analysis in cylindrical coordinates is the excitation of the cavity modes directly from the membrane motion. Figure 11 shows the pressure in a curved cavity with no channels excited by an axially moving spherical cap.

Unlike the planar piston the resulting volume velocity is not orthogonal to the modes and the cavity resonances are excited.

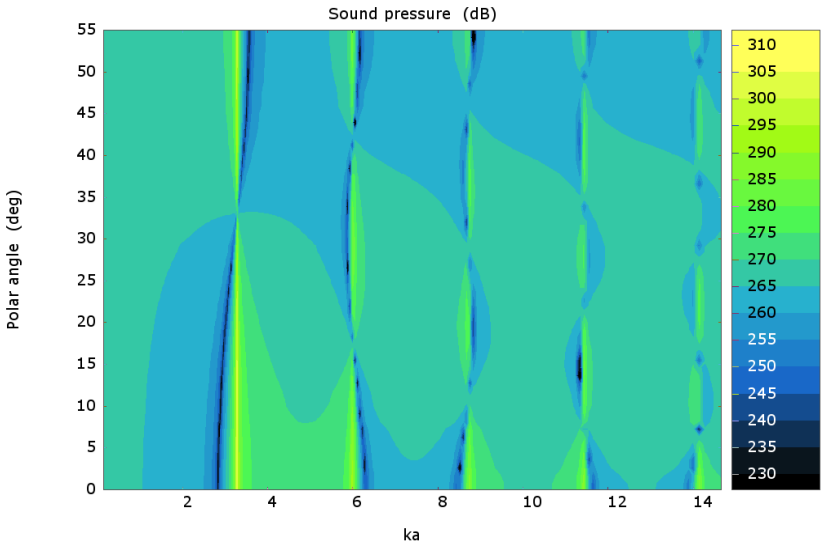

Figure 11: FEM model of curved cavity, no channels, rigid axially moving membrane.

4 SUPPRESSION OF MODES BY BALANCING CHANNEL AND MEMBRANE EXCITATION

In order to improve upon Smiths method for setting channel geometry, it is necessary to analyse the behaviour of the membrane, cavity and channels in a spherical coordinate system. This allows a closer representation to the practical reality since the cavity and membrane are spherical caps just as in real compression drivers.

Conceptually, the approach is similar to Smiths. All excitation of the cavity modes is synthesized such that the overall pressure variation in the cavity is zero.

The cavity is analysed in a spherical coordinate system, approximating the geometry as shown in Figure 16.

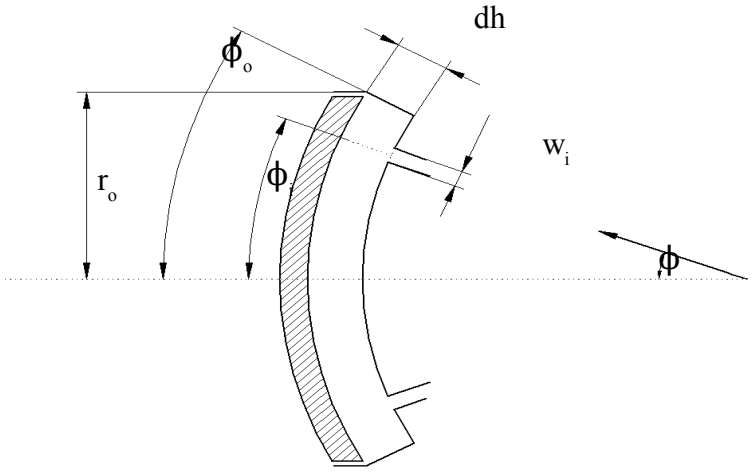

Figure 12: Spherical representation of compression driver.

The common notation used to describe a spherical coordinate system is that of Zwillinger[6] as depicted in Figure 13. In this work we replace the symbol for the radial coordinate, r, with h so we avoid confusion with the radial coordinate in the cylindrical coordinate system, to which we shall still refer.

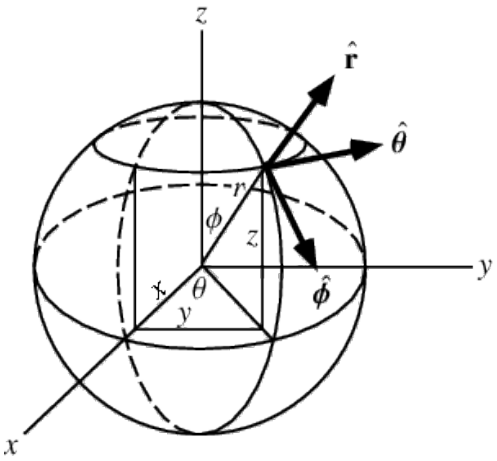

Figure 13: Spherical coordinate system notation.

We start from the homogeneous Helmholtz equation[7] in equation 1 and first consider the acoustical behaviour of the undriven rigid-walled compression cavity.

$$\nabla^2 p + \frac{\omega^2}{c_o^2} p = 0 \tag{1}$$

In spherical coordinates the Laplacian can be written as shown below[8] in equation 2.

$$\nabla^2 p = \frac{\partial^2 p}{\partial h^2} + \frac{2}{h}\frac{\partial p}{\partial h} + \frac{1}{h^2 \sin^2 \phi}\frac{\partial^2 p}{\partial \theta^2} + \frac{1}{h^2}\frac{\partial^2 p}{\partial \phi^2} + \frac{\cos \phi}{h^2 \sin \phi}\frac{\partial p}{\partial \phi} \tag{2}$$

Solutions can be found using the method of separation of variables[7,9].

$$p(h,\theta,\phi,t) = H(h)\Theta(\theta)\Phi(\phi)T(t) \tag{3}$$

$$T(t) = T_1 e^{-j\omega t} + T_2 e^{j\omega t} \tag{4}$$

$$\Phi(\phi) = \Phi_1 P_l^m(\cos\phi) + \Phi_2 Q_l^m(\cos\phi) \tag{5}$$

$$\Theta(\theta) = \Theta_1 e^{-jm\theta} + \Theta_2 e^{jm\theta} \tag{6}$$

$$H(h) = H_1 j_l(kh) + H_2 y_l(kh) \tag{7}$$

With $T_1, T_2, \Phi_2, \Phi_2, \Theta_1, \Theta_2, H_1 \& H_2$ as arbitrary constants. P_l^m and Q_l^m in equation 5 are Legendre functions of the first and second kinds respectively[10]. j_l and y_l in equation 7 are spherical Bessel functions of the first and second kind respectively[11,12].

In order to effectively apply this general solution of the wave equation to the situation at hand we first make some simplifications.

Selecting our convention for time dependence, we set $T_2 = 0$.

The compression cavity is totally axisymmetric in both geometry and excitation. We are not interested in pressure variations occurring in θ . In the driven case, the circumferential function $\Theta(\theta)$ has only trivial solutions in our frequency band of interest and so we set $m = 0, \Theta_1 + \Theta_2 = 1$ such that $\Theta(\theta) = 1$.

The compression cavity is small in h and in the frequency band of interest only trivial behaviour is observed. We simplify $H(h)=1$.

The Legendre function of the second kind, Q_l^m , appearing in the polar function, is singular at $\cos\phi=1$. Constraining the pressure in the compression cavity to be finite we set $\Phi_2=0$.

Our simplified solution to the wave equation in the rigid walled compression cavity is

$$p(\phi,t)=A_1 P_l(\cos\phi)\,e^{-j\omega t} \tag{8}$$

The pressure must obey the rigid wall boundary condition at the diameter of the cavity as described in equation 9.

$$\frac{dp}{d\phi}=0\Big|_{\phi=\phi_0} \tag{9}$$

To resolve this condition we require that

$$\frac{dP_l(\cos\phi)}{d\phi}=0\Big|_{\phi=\phi_0} \tag{10}$$

This requirement is met by choice of l . Hoersch demonstrates that a Legendre function of the first kind may be approximately described as a summation of Bessel functions[13]. Using his expression for the Legendre function it is possible to analytically derive an infinite set of values of l_n satisfying equation 10 in terms of a summation of Bessel function roots.

These values of l_n give the eigenvalues of the system as shown in equation 11. This expression is derived from comparison of our simplified wave equation in spherical coordinates with the Legendre differential equation[10].

$$k_n^2 \;=\; l_n\left(l_n+1\right)h_o^{-2} \;\;,\;\; \omega_n=k_n c_o \tag{11}$$

The eigenfunctions of the cavity are given by inserting the values of l_n into the expression for the spatial pressure variation in the cavity, equation 8.

$$\Psi_n(\phi)=A_n P_{l_n}(\cos\phi) \tag{12}$$

The normalisation term, A_n , is chosen to satisfy equation 13.

$$\int_V \Psi_n(\phi)^2\,dV=V \tag{13}$$

Hoerch's Bessel summation description of Legendre functions is approximate and only valid for a small range of x and l , to improve the accuracy of the computation FEM derived values of ω_n and $\Psi_n(\phi)$ are actually used for all numerical calculations in this work.

4.1 Analysis of the Driven Behaviour of the Cavity

The pressure in a undamped, driven acoustical cavity excited by motion of it's walls can be described in terms of the rigid walled eigenfunctions and eigenfrequencies[14,7].

$$p(\boldsymbol{x}) = \sum_{n=0}^{\infty} \frac{j\omega\rho_o \Psi_n(\boldsymbol{x})}{V\left[k_n^2 - k^2\right]} \int_s \Psi_n(\boldsymbol{y}) u(\boldsymbol{y}) . \boldsymbol{n}\, dS \tag{14}$$

The choice of normalisation, equation 13, is important for the use of this expression[14].

4.1.1 Behaviour without exit channels

We first look at the case were the cavity is driven by an axially moving membrane on one side of the cavity but otherwise there is no other surface normal velocity. In this case we need only perform the integral in equation 14 over the surface of the membrane.

$$\int_s \Psi_n(\boldsymbol{y}) u(\boldsymbol{y}) . \boldsymbol{n}\, dS = \int_{\phi=0}^{\phi_o} \Psi_n(\phi) u_o \cos\phi\, dS \tag{15}$$

This is now easily evaluated by change of variables as shown below.

$$\frac{dS}{d\phi} = \frac{\pi r_o^2}{\sin^2\phi_o} 2\sin\phi \quad , \qquad 2\sin\phi\cos\phi = \sin(2\phi)$$

[15]

$$\int_{\phi=0}^{\phi_o} \Psi_n(\phi) u_o \cos\phi\, dS = \frac{u_o \pi r_o^2}{\sin^2\phi_o} \int_{\phi=0}^{\phi_o} \Psi_n(\phi) \sin(2\phi)\, d\phi \tag{16}$$

For the particular case $n=0$ we can evaluate the integral easily as $\Psi_0(\phi)=1$.

$$\frac{u_o \pi r_o^2}{\sin^2\phi_o} \int_{\phi=0}^{\phi_o} \sin(2\phi)\, d\phi = u_o \pi r_o^2 \tag{17}$$

Inserting equations 16 and 17 into 14, we can write an expression for the pressure in the cavity.

$$p_m(\phi) = \frac{\rho_o c_o^2}{V} \frac{u_o \pi r_o^2}{j\omega} + \sum_{n=1}^{\infty} \frac{j\omega\rho_o \Psi_n(\phi)}{V\left[k_n^2 - k^2\right]} \frac{u_o \pi r_o^2}{\sin^2\phi_o} \int_{\hat{\phi}=0}^{\phi_o} \Psi_n(\hat{\phi}) \sin(2\hat{\phi})\, d\hat{\phi} \tag{18}$$

It is useful to separate the zero[th] term in the summation, as shown, as this contains the desirable lumped behaviour. Comparison of this expression with the equivalent for the Bob Smith cylindrical geometry reveals an important detail. With the cylindrical approximation of the geometry, the diaphragm velocity does not excite any of the cavity modes with the exception of the desirable zero[th] mode. The Smith slot geometry derivation continues assuming that all cavity mode excitation is due to the acoustic velocity at the channels. However, we see with this result that in the spherical geometry, the motion of the dome itself also excites the compression cavity modes. As the spherical geometry is a more accurate representation of the real compression driver geometry this is an important detail and any modal suppression method should take this excitation into account.

4.1.2 Behaviour with exit channels

In addition to the radiating membrane on the entrance side of the compression cavity, in a fully assembled driver there is also acoustical velocity on the opposite exit side occurring due to the motion of air entering and leaving the phase plug channels.

The exit side surface normal velocity is represented by the function $u_e(\phi)$. If we make the approximation that the phase plug channels are sufficiently narrow that they can be considered to only impart velocity on the cavity at discrete locations, we can then write $u_e(\phi)$ as below making use of the Dirac delta function[16].

$$u_e(\phi)=w_1 u_1 \delta(\phi-\phi_1)+w_2 u_2 \delta(\phi-\phi_2)+...+w_N u_N \delta(\phi-\phi_N) \tag{19}$$

In this expression, u_N refers to the acoustical velocity entering the cavity at channel N. w_N is the width of the Nth channel. The motivation for this simplification is to make the exit velocity function easy to integrate over the surface of the phase plug cavity.

As before we use equation 14 to provide us with an expression for the acoustical pressure in the compression cavity. We need not re-analyse the effect of the radiating membrane, which was considered in the previous chapter, instead we assume that the total pressure in the cavity can be described as the sum of two pressure contributions: one occurring because of the volume velocity of the radiating membrane, p_m , and the other because of the channel entrance acoustical velocity, p_c .

$$p=p_m+p_c \tag{20}$$

We already have the result for p_m in equation 18.

p_c is evaluated using the same summation of eigenfunctions as was applied previously.

$$p_c(\phi)=\sum_{n=0}^{\infty} \frac{j\omega\rho_o \Psi_n(\phi)}{V\left[k_n^2-k^2\right]} \int_{\hat{\phi}=0}^{\phi_o} \Psi_n(\hat{\phi}) u_e(\hat{\phi})\, dS \tag{21}$$

The integral in this expression can be easily evaluated using the sifting property of the delta function.

$$\int_{\hat{\phi}=0}^{\phi_o} \Psi_n(\hat{\phi}) u_e(\hat{\phi})\, dS=\sum_{i=1}^{N} \Psi_n(\phi_i) A_i u_i \tag{22}$$

Where A_i is the area of the ith channel entrance.

Inserting 22 into 21 we have an expression for part for the pressure excited by motion of air in the channel entrances.

$$p_c(\phi)=\sum_{n=0}^{\infty} \frac{j\omega\rho_o \Psi_n(\phi)}{V\left[k_n^2-k^2\right]} \sum_{i=1}^{N} \Psi_n(\phi_i) A_i u_i \tag{23}$$

This can be combined with equation 18 to give the full pressure due to the channel motion and the membrane motion.

$$p(\phi)=\sum_{n=0}^{\infty} \frac{j\omega\rho_o \Psi_n(\phi)}{V\left[k_n^2-k^2\right]} \left[\frac{u_o \pi r_o^2}{\sin^2\phi_o} \int_{\hat{\phi}=0}^{\phi_o} \Psi_n(\hat{\phi}) \sin(2\hat{\phi})\, d\hat{\phi}+\sum_{i=1}^{N} \Psi_n(\phi_i) A_i u_i \right] \tag{24}$$

4.1.3 Suppression of Modal excitation by Channel Arrangement

We now can use equation 24 as a starting point to derive a channel geometry to minimise the excitation of the acoustical modes in the compression cavity. Extracting the n=0 terms from the summation in 24 we separate the zero[th] mode from the other excitation.

$$p(\phi)=\frac{\rho_o c_o^2}{j\omega V}\left(u_o \pi r_o^2+\sum_{i=1}^{N} A_i u_i\right)+\ldots \\ \sum_{n=1}^{\infty}\frac{j\omega\rho_o \Psi_n(\phi)}{V\left[k_n^2-k^2\right]}\left[\frac{u_o \pi r_o^2}{\sin^2\phi_o}\int_{\hat{\phi}=0}^{\phi_o}\Psi_n(\hat{\phi})\sin(2\hat{\phi})\,d\hat{\phi}+\sum_{i=1}^{N}\Psi_n(\phi_i)A_i u\right. \tag{25}$$

This is a very useful manipulation as it separates the desired lumped behaviour from the undesirable higher order excitation.

From here it is clear that in order to suppress the excitation of the m[th] mode, we require that

$$u_o \pi r_o^2 \zeta_m+\sum_{i=1}^{N}\Psi_m(\phi_i)A_i u_i=0 \tag{26}$$

Where

$$\zeta_m=\frac{1}{\sin^2\phi_o}\int_{\hat{\phi}=0}^{\phi_o}\Psi_n(\hat{\phi})\sin(2\hat{\phi})\,d\hat{\phi} \tag{27}$$

This expression is quite similar to that in equation for the cylindrical geometry but with an additional term, ζ_m , representing the modal excitation due to the diaphragm motion.

The integral expression giving ζ_m can be calculated explicitly for each mode of the cavity. This can be done analytically, perhaps using the Hoersch expression for the eigenfunctions, or numerically.

Equation 26 requires us to know both the diaphragm velocity, u_o , and also the slot velocities, u_i , before we can ensure that undesirable modal excitation is suppressed. This is a similar situation to that encountered by Smith when he assumes that the velocities of each slot are identical. Though not entirely rigorous, we take a parallel approach and make the assumption that our final compression driver behaves like the lumped terms in equation 25.

$$p=\frac{\rho_o c_o^2}{j\omega V}\left(u_o \pi r_o^2+\sum_{i=1}^{N} A_i u_i\right) \tag{28}$$

The velocities at the channel entrances can be related to the cavity pressure at the channel entrance by the specific acoustical impedance of the channels.

$$u_i=\frac{p}{z_i} \tag{29}$$

Unfortunately, unlike the cylindrical situation, it is not sufficient for us to assume that the channel impedances are the same. We not only require the channel velocities to be identical but be must

also know their value in relation to the diaphragm velocity, hence we need to know the channel impedances. This is a little problematic, the channel impedance is dependent upon the horn to which the driver is connected. Happily, while the impedance of the channel is likely to vary at the lower end of the driver bandwidth, due to the cut-on characteristic of the attached horn, at the upper end, where the acoustical resonances in the cavity are problematic, the channel specific acoustical impedance will in most cases very close to $\rho_o c_o$. Inserting this into 28 we have

$$u_i\left(\frac{j\omega V}{c_o \pi r_o^2}-\frac{A_T}{\pi r_o^2}\right)=u_o \tag{30}$$

Where

$$A_T=\sum_{i=1}^{N} A_i \tag{31}$$

From equation 30 we can see that the real parts of the velocities are related by the compression ratio as we might expect. The imaginary part presents us with a problem. The acoustical modes in the cavity are excited by the motion of the dome and of the air entering the channels. We intend to arrange these velocities such that the excitation occurring because of the dome motion is compensated by the excitation occurring because of the channel air motion. We can only expect to achieve this when the two velocities are in-phase with each other. There is nothing that can be done to suppress excitation from the dome which occurs in quadrature to the excitation from the channels. The quadrature component is a result of the compliance of the air in the compression cavity. This is an effect which is also problematic in other areas, when the compliance becomes significant the channel velocity magnitude is reduced compared to the dome motion and the output of the driver is reduced. The compliance sets the upper bandwidth on the compression driver output. This effect is well known, the practical solution to the problem is to keep the volume of the compression cavity to a minimum. We can approximate equation 30 in terms of the width of the compression cavity.

$$u_i\left(\frac{j\omega dh}{c_o}-\frac{A_T}{\pi r_o^2}\right)\approx u_o \tag{32}$$

Modern compression drivers, built with carefully designed and constructed parts, have extremely small cavity widths (dh) in order to keep the compliance problem to a minimum. Typically dh is in the range 0.3-0.6mm in a modern compression driver. With a normal compression driver design equation 30 is dominated by the real term, the imaginary term is small over the bandwidth of operation, for our requirements it is sufficient to make the approximation that the velocities are related by only the real part.

$$u_i\frac{-A_T}{\pi r_o^2}\approx u_o \tag{33}$$

Substituting this result into equation 26 we can write the requirement for modal suppression as

$$\sum_{i=1}^{N} \Psi_m(\phi_i)\, A_i = A_T \zeta_m \tag{34}$$

Rearranging this so that all terms appear on the left hand side within the summation, using equation 31, we have.

$$\sum_{i=1}^{N} \left(\Psi_m(\phi_i) - \zeta_m \right) A_i = 0 \tag{35}$$

This condition can be met for specific modes by careful selection of the channel positions, ϕ_i , and entrance areas, A_i . If we have N channels it is possible to meet the condition for N modes. As with the Bob Smith case we choose the lowest N in order to extend the lumped behaviour to as high a frequency as possible

The condition can then be written as a set of N simultaneous equations which can be solved by writing in matrix form as shown below.

$$\begin{bmatrix} \Psi_1(\phi_1)-\zeta_1 & \Psi_1(\phi_2)-\zeta_1 & \Psi_1(\phi_3)-\zeta_1 & \cdots & \Psi_1(\phi_N)-\zeta_1 \\ \Psi_2(\phi_1)-\zeta_2 & \Psi_2(\phi_2)-\zeta_2 & \Psi_2(\phi_3)-\zeta_2 & \cdots & \Psi_2(\phi_N)-\zeta_2 \\ \Psi_3(\phi_1)-\zeta_3 & \Psi_3(\phi_2)-\zeta_3 & \Psi_3(\phi_3)-\zeta_3 & \cdots & \Psi_3(\phi_N)-\zeta_3 \\ \vdots & \vdots & \vdots & \ddots & \vdots \\ \Psi_N(\phi_1)-\zeta_N & \Psi_N(\phi_2)-\zeta_N & \Psi_N(\phi_3)-\zeta_N & \cdots & \Psi_N(\phi_N)-\zeta_N \end{bmatrix} \begin{bmatrix} A_1 \\ A_2 \\ A_3 \\ \vdots \\ A_N \end{bmatrix} = \begin{bmatrix} 0 \\ 0 \\ 0 \\ \vdots \\ 0 \end{bmatrix} \tag{36}$$

There are non-trivial solutions when the square matrix on the left has a determinant of zero. As in the Smith case, we manipulate this equation into an easier to solve form by eliminating a row. In this case we choose the channel positions, ϕ_i , such that.

$$\Psi_N(\phi_i) = \zeta_N \tag{37}$$

This means that the N[th] row of the matrix in equation 36 is zero. The equations can then be rearranged to give.

$$\begin{bmatrix} \Psi_1(\phi_2)-\zeta_1 & \Psi_1(\phi_3)-\zeta_1 & \cdots & \Psi_1(\phi_N)-\zeta_1 \\ \Psi_2(\phi_2)-\zeta_2 & \Psi_2(\phi_3)-\zeta_2 & \cdots & \Psi_2(\phi_N)-\zeta_2 \\ \vdots & \vdots & \ddots & \vdots \\ \Psi_{N-1}(\phi_2)-\zeta_{N-1} & \Psi_{N-1}(\phi_3)-\zeta_{N-1} & \cdots & \Psi_{N-1}(\phi_N)-\zeta_{N-1} \end{bmatrix} \begin{bmatrix} A_2/A_1 \\ A_3/A_1 \\ \vdots \\ A_N/A_1 \end{bmatrix} = \begin{bmatrix} \zeta_1-\Psi_1(\phi_1) \\ \zeta_2-\Psi_2(\phi_1) \\ \vdots \\ \zeta_{N-1}-\Psi_{N-1}(\phi_1) \end{bmatrix} \tag{38}$$

Equation 38 is easily soluble by inversion of the square matrix.

For example in the case of a three channel phase plug with $\phi_o = 55^o$ we can calculate.

$$\begin{aligned} \zeta_1 &= 0.0624392 \\ \zeta_2 &= -0.012609 \\ \zeta_3 &= 0.0048689 \end{aligned} \tag{39}$$

We then choose our channel positions, according to equation 37, to be.

$$\begin{aligned} \phi_1 &= 0.2350\,\phi_o \\ \phi_2 &= 0.5431\,\phi_o \\ \phi_3 &= 0.8476\,\phi_o \end{aligned} \tag{40}$$

The simultaneous equations can then be solved to find the channel area ratios.

$$\frac{A_2}{A_1}=2.0158$$
$$\frac{A_3}{A_1}=2.2649 \quad (41)$$

Which can be equivalently written as channel width ratios.

$$\frac{w_2}{w_1}=0.9056$$
$$\frac{w_3}{w_1}=0.6973 \quad (42)$$

The curved cavity was also analysed using a parametrized FEM model. Among the parameters of the model were the design variables in which we are interested: the position and area of the channels. An optimization was used to minimize the difference between the three channel pressures. In both cases very similar results were obtained. Unlike the Smith design guidelines, the channel geometry is dependent upon the angle of the membrane and cavity. The degree to which the membrane itself excites the cavity modes is dependent upon the cavity angle. The new design method tends towards the Smith guidelines as the angle of the cavity curvature is decreased and the flat, cylindrical situation is approached.

55 degree	Flat disc
0.235 θ_0	0.238 r_o
0.543 θ_0	0.543 r_o
0.848 θ_0	0.853 r_o

Table 1: Comparison of channel positions for a three channel design having a 55 degree curved cavity and a flat cavity.

55 degree	Flat disc
1	1
0.9056	1.025
0.6973	1.065

Table 2: Comparison of channel width for a three channel design having a 55 degree curved cavity and a flat cavity.

It may be observed from tables 1 and 2 that the change in the calculated widths of the channels is much larger than the change in the positions. In both cases, we position our channels to be very close to the nodal lines of the N^{th} cavity mode: the similarity in positioning highlights that in both cases the mode shape is very similar and these nodal lines occur in roughly the same position around the cavity.

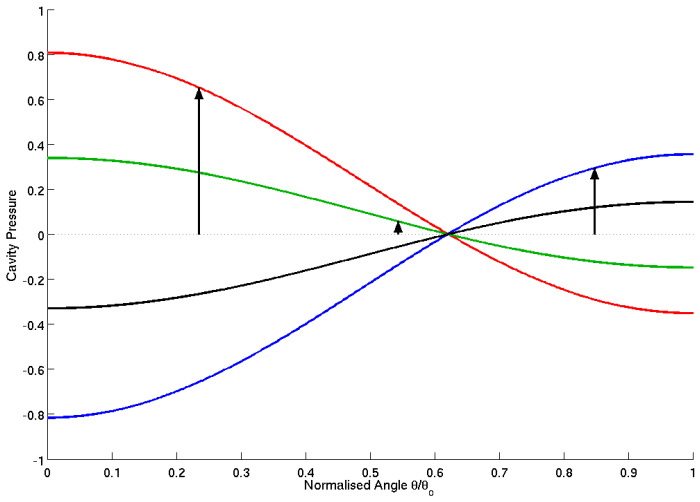

Figure 14: Pressure excited by each channel and membrane (black line), first mode.

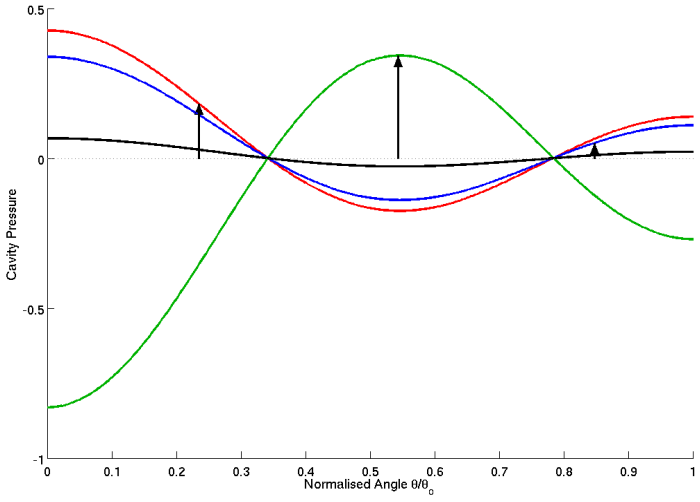

Figure 15: Pressure excited by each channel and membrane (black line) , second mode.

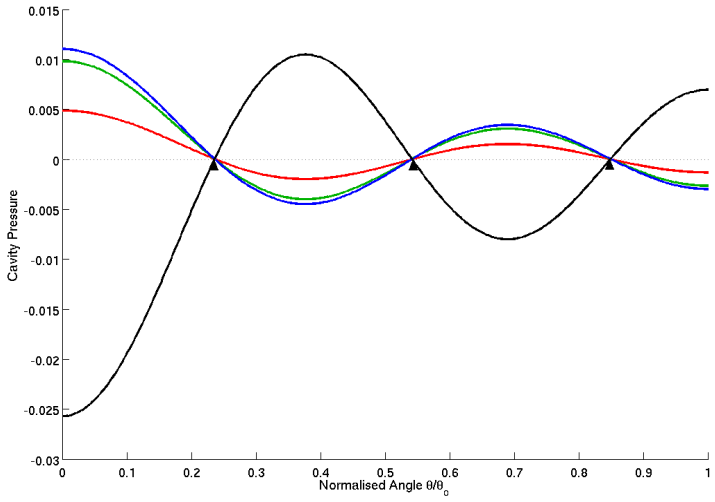

Figure 16: Pressure excited by each channel and membrane (black line) , third mode.

Being a little more precise, with the new design method the target is, in fact, not to place the channels in *exactly* the nodal positions but, as with the lower modes, to compensate for the excitation by the membrane. The channels are placed slightly away from the nodal lines. However, this shift is very small as inevitably the channels excite the N^{th} mode constructively, additionally the membrane modal excitation reduces with higher modes: only a minute shift is required to match the channel excitation to the membrane excitation. In practice, it is not clear if the best solution is to attempt to suppress the N^{th} mode or to simply decouple the channels from it and aim positionally directly for the nodal lines. This is largely academic with any reasonable dome angle and the cases N>1. In practical terms the positional difference is minute, as can be seen from Table 1. For the case N=1, however, this question remains.

It is helpful to graphically look at the modal excitation for each term of the summation in equation 25 which we have attempted to suppress. These are equivalent figures to those presented in Smith's paper except for the addition of a contribution to the figure from the excitation due to the dome motion. Figure 14, 15 and 16 are for the 1^{st}, 2^{nd} and 3^{rd} modes respectively.

Figure 17 shows the pressures in the three channels calculated by an FEM model of the same curved cavity as in Figure 10 with channels arranged using the new design method. A good improvement in the regularity of the pressure in each of the channels can be observed.

It is interesting to note that it is not possible to synthesize a design to work as well in the curved cavity as can be achieved in the flat disc case, Figure 9. With the flat disc cavity, it is not necessary to link the channel velocity to the membrane velocity as all excitation of modes is by the channels. With the curved case, this added complication results in a small quadrature component between the channel and membrane velocity that cannot be suppressed. Additionally, it is very safe to assume that, in the case of the flat disc, the acoustical impedance of each of the channels is the same; however, this is certainly a less accurate assumption in the curved case as the channels themselves are forced to have some curvature. Nevertheless, it is clear that the assumptions made in the analytical analysis are quite reasonable because of the good agreement with the optimized FEM results.

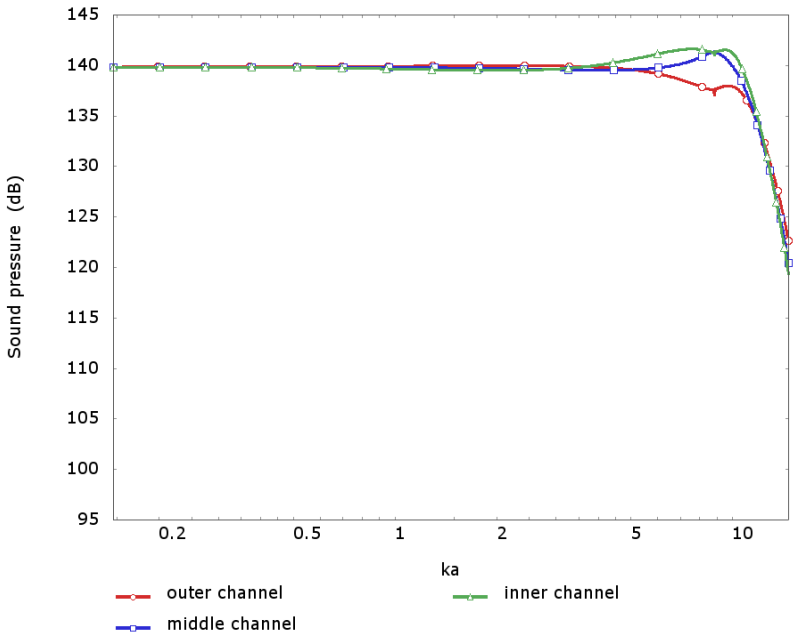

Figure 17: Spherical cavity with channel position and width derived by new approach.

5 APPLICATION TO PRACTICAL COMPRESSION DRIVER.

The approach described in this paper was developed during the design of a 1.4 Inch diameter exit compression driver. This driver has a 3 inch voice coil wound with copper-clad aluminium wire on to a glass filled polyamide former. The former is coupled to a titanium membrane, which is supported by a polyamide surround.

The acoustic FEM model used in the driver development includes most physical detail. The mesh used was associatively linked to a parametrized solid model. This allowed most aspects of the design to be readily varied. For example channel position, width and length were all controlled by parameters in addition to many other aspects of the design. Mechanical parts are all flexible and are coupled to the acoustical parts of the model.

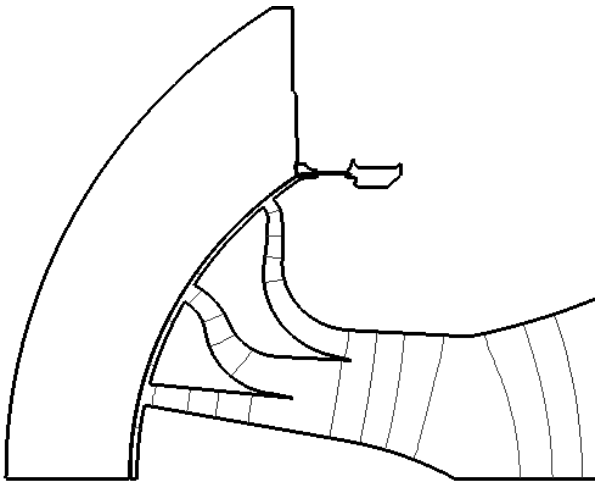

Figure 18: FEM model of final design on horn showing iso-pressure contours at 8,417Hz.

The final phase-plug design is illustrated in Figure 18 mounted on a horn.

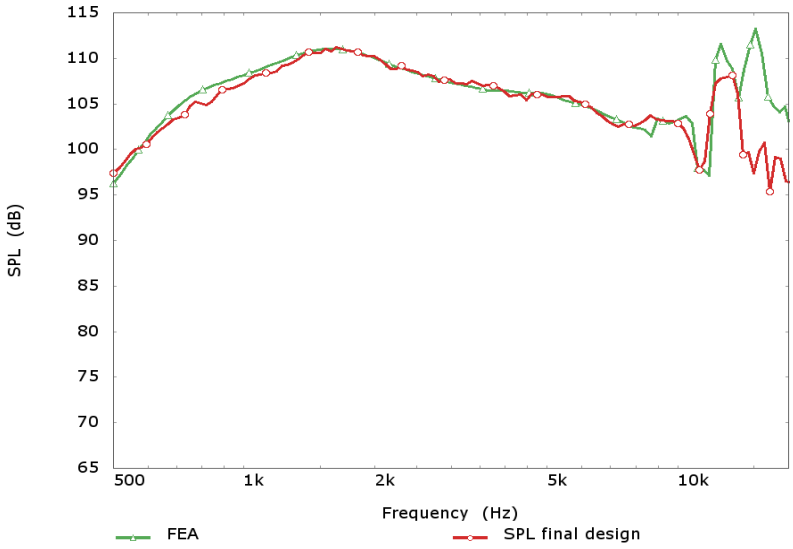

Figure 19: FEM versus measured frequency response on axisymmetric horn.

Many FEM models of other domains were used, static magnetic for magnet design. Magneto-dynamic for copper sleeve design and derivation of blocked impedance of voice coil. The use of these other FEM techniques to derive a frequency response of a driver are described in an earlier paper[17]. Additionally, large displacement analysis was used to evaluate the compliance variation

with diaphragm displacement due to the surround resulting in the choice of a small surround with a single roll.

The horn mounted axial response of the final driver at 1m along with the FEM prediction is shown in Figure 19.

6 DISCUSSION

This work, by necessity rather than intention, has resulted in an interesting counterpoint of analytical and computational analysis.

FEM used as a tool to get at the behaviour by splitting the problem/design into abstract experiments.

Analytical analysis helps to confirm the physics and that the optimum solution is reached. It also makes it possible to generalize (for example for many angles). For some cases with too many degrees of freedom there is no alternative.

FEM can, of course, go further and attempt to find solutions for more complex cases such as optimum positions and widths of channels when the membrane is not rigid or cavity and membrane shapes that cannot be described by separable coordinate systems.

Computational analysis is not, however, required to understand that the cylindrical representation is not a sufficient description of the problem considered. Though, conversely, the analytical analysis of the spherical case is complicated by the presence of Legendre functions of non-integer order and integrals of these functions. Issues dealing with such expressions are neatly sidestepped as happily we are able to insert a little numerical analysis when other routes fail. The Eigenfunctions used in the analysis are, in fact, calculated with FEM models.

The traditional analytical analysis approach of reducing a problem into easy-to-understand simply behaving parts is a truly powerful way of applying FEM modelling. The parts can be analysed and conquered individually. Assumptions can be checked and the parts re-assembled after they are understood.

7 CONCLUSIONS

The equal path-length approach does not take into account the modal behaviour and cannot be expected to produce optimum results in every case. Smith's methodology is very successful with the flat disc shaped cavity giving almost total suppression of the modes. However, when applied to a cavity shaped like a spherical cap Smith's technique does not produce such good results; While for the planar membrane, the channels alone excite the modes; the spherical cap membrane excites the modes even in the absence of channels.

In this paper it is demonstrated that the correct choice of channel widths and positions can compensate for the normal volume velocity variation of the membrane and avoid exciting modes.

8 REFERENCES

1. E. Wente and A. Thuras, "Moving Coil Telephone Receivers And Microphones," *The Journal of the Acoustical Society of America*, vol. 3, no. 1A, pp. 44-55, Jul 1931.
2. PACSYS Ltd., *Pafec Acoustics - User Manual Level 8.8*. Strelley Hall Nottingham NG8 6PE: PACSYS Ltd., 2008.
3. C. A. Henricksen, "Phase Plug Modelling And Analysis: Radial Versus Circumferential Types," presented at The 59th Convention of the AES, preprint 1328, Feb 1978.
4. B. H. Smith, "An Investigation Of The Air Chamber Of Horn Type Loudspeakers," *The Journal of the Acoustical Society of America*, vol. 25, no. 2, pp. 305-312, Mar 1953.
5. F. Murray, "An Application Of Bob Smith'S Phasing Plug," presented at the 61st convention of the AES, preprint 1384, Oct 1978.
6. D. Zwillinger, *Spherical Coordinates In Space*. Boca Raton, FL: CRC Press, 1995.
7. E. G. Williams, *Fourier Acoustics - Sound Radiation And Nearfield Acoustical Holography*. 24-28 Oval Road, London, NW1 7DX: Academic Press, 1999.
8. E. W. Weisstein "Spherical Coordinates," *From MathWorld-A Wolfram Web Resource* [Online]. Available: http://mathworld.wolfram.com/SphericalCoordinates.html [Accessed Jul. 2007].
9. J. Renze and E. W. Weisstein "Separation Of Variables," *MathWorld - A Wolfram Web Resource* [Online]. Available: http://mathworld.wolfram.com/SeparationofVariables.html [Accessed Mar. 2008].
10. E. W. Weisstein "Legendre Differential Equation," *From MathWorld - A Wolfram Web Resource* [Online]. Available: http://mathworld.wolfram.com/LegendreDifferentialEquation.html [Accessed Jul. 2007].
11. E. W. Weisstein "Spherical Bessel Function Of The First Kind," *MathWorld - A Wolfram Web Resource* [Online]. Available: http://mathworld.wolfram.com/SphericalBesselFunctionoftheFirstKind.html [Accessed Jul. 2008].
12. E. W. Weisstein "Spherical Bessel Function Of The Second Kind," *MathWorld - A Wolfram Web Resource* [Online]. Available: http://mathworld.wolfram.com/SphericalBesselFunctionoftheSecondKind.html [Accessed Jul. 2008].
13. V. A. Hoersch, "Non-Radial Harmonic Vibrations Within A Conical Horn," *Physics Review*, vol. 25, no. 2, pp. 218-224, Feb 1925.
14. P. A. Nelson and S. J. Elliot, *Active Control Of Sound*. London: Academic Press, 1992.
15. E. W. Weisstein "Double-Angle Formulas," *MathWorld - A Wolfram Web Resource* [Online]. Available: http://mathworld.wolfram.com/Double-AngleFormulas.html [Accessed Jul. 2008].
16. E. W. Weisstein "Delta Function," *MathWorld - A Wolfram Web Resource* [Online]. Available: http://mathworld.wolfram.com/DeltaFunction.html [Accessed May. 2008].
17. M. Dodd, "The Development Of A Forward Radiating Compression Driver By The Application Of Acoustic, Magnetic And Thermal Finite Element Methods," presented at The 115th Convention of the AES, preprint 5886, Oct 2003.